MNRAS **435,** 1451–1462 (2013)
Advance Access publication 2013 August 16
doi:10.1093/mnras/stt1386

A small survey of the magnetic fields of planet-host stars ⋆

R. Fares,[1]† C. Moutou,[2] J.-F. Donati,[3] C. Catala,[4] E. L. Shkolnik,[5] M. M. Jardine,[1] A. C. Cameron[1] and M. Deleuil[2]

[1]*School of Physics and Astronomy, University of St Andrews, St Andrews KY16 9SS, UK*
[2]*Aix Marseille Université, CNRS, LAM, UMR 7326, F-13388 Marseille, France*
[3]*IRAP-UMR 5277, CNRS & Univ. de Toulouse, 14 Av. E. Belin, F-31400 Toulouse, France*
[4]*Observatoire de Paris, 61 avenue de l'Observatoire, F-75014 Paris, France*
[5]*Lowell Observatory, 1400 West Mars Hill Road, Flagstaff, AZ 86001, USA*

Accepted 2013 July 23. Received 2013 July 22; in original form 2013 May 30

ABSTRACT

Using spectropolarimetry, we investigate the large-scale magnetic topologies of stars hosting close-in exoplanets. A small survey of 10 stars has been done with the twin instruments Télescope Bernard Lyot /NARVAL and Canada–France–Hawaii Telescope/ESPaDOnS between 2006 and 2011. Each target consists of circular polarization observations covering 7–22 d. For each of the seven targets in which a magnetic field was detected, we reconstructed the magnetic field topology using Zeeman–Doppler imaging. Otherwise, a detection limit has been estimated. Three new epochs of observations of τ Boo are presented, which confirm magnetic polarity reversal. We estimate that the cycle period is 2 yr, but recall that a shorter period of 240 d cannot still be ruled out. The result of our survey is compared to the global picture of stellar magnetic field properties in the mass–rotation diagram. The comparison shows that these giant planet-host stars tend to have similar magnetic field topologies to stars without detected hot Jupiters. This needs to be confirmed with a larger sample of stars.

Key words: techniques: polarimetric – stars: activity – stars: individual – stars: magnetic field – planetary systems.

1 INTRODUCTION

The role of the stellar magnetic field in the evolution of stellar and planetary systems is suspected to be important, but poorly constrained by observations. For instance, stellar magnetic braking, planet migration and dynamical evolution may be acting simultaneously in the early stages of evolution of the systems, with an impact on the final state that depends on the system properties (Dobbs-Dixon, Lin & Mardling 2004; Lai, Foucart & Lin 2011). In the case of short-period planets, the interactions between the planet and the star continue throughout the lifetime of the system, as the planet may be embedded in the magnetosphere of the star at only a few stellar radii from the star's surface. The impact of the stellar wind may then be important (Vidotto et al. 2012), and even reconnections between the stellar and planetary magnetic fields could happen (Cohen et al. 2010, 2011; Lanza 2012). This can influence the planetary magnetic field, the planetary upper atmosphere and maybe the internal structure of the planet as well. On the stellar side, the close-in planet, especially when it is massive, may induce anomalies on the stellar surface through magnetic interactions (Shkolnik, Walker & Bohlender 2003; Shkolnik et al. 2005; Walker et al. 2008; Pagano et al. 2009), although several observational searches for such signatures give results that are either unconfirmed, intermittent or difficult to interpret (e.g. Cranmer & Saar 2007; Shkolnik et al. 2008; Fares et al. 2012). In order to better understand the environment where a close-in planet orbits its star, it is necessary to have information about the stellar magnetic field topology. Then, extrapolation techniques may be used to get quantified properties of the magnetic environment that may impact the planet (Jardine, Collier Cameron & Donati 2002; Fares et al. 2010, 2012).

In this paper, we investigate the large-scale magnetic properties of 10 planet-host stars using spectropolarimetric observations, in order to provide inputs to (1) more intensive similar campaigns on stars where the magnetic field is strong enough for an accurate characterization and (2) extrapolation models that explore the star–planet magnetic interactions. Three new epochs of observations are reported for the short-cycle τ Boo star, which makes eight the total number of epochs when we observed this star. In Section 2, we describe the observational method and material, in Section 3, we present the stellar sample and in Section 4, we discuss the results before concluding.

2 OBSERVATIONS

We have secured spectropolarimetric observations of stars hosting close-in extrasolar planets, using either ESPaDOnS at the

⋆ Based on observations obtained by NARVAL at Télescope Bernard Lyot (CNRS) and ESPaDOnS at Canada–France–Hawaii telescope.
† E-mail: rf60@st-andrews.ac.uk

Table 1. Summary of observations and results presented in this paper. The instrument used is either CFHT/ESPaDOnS (ESP) or TBL/NARVAL (NAR). The epochs of observations and numbers of spectra (# seq) are listed. Detection status is N: no detection, Y: few detections, M: several detections and map reconstruction. The mean magnetic field strength (B), the percentage of poloidal energy over total magnetic energy (Pol) and the percentage of axisymmetry in the poloidal field are given for all epochs. When there is no detection, an upper limit is given for B for an adopted peculiar magnetic topology (and thus poloidal contribution).

Name	Instrument	Date	# seq	Detection	B (G)	Pol (per cent)	Axisy (per cent)	Ref.
HD 46375	ESP	Jan 08	10	Y–M	2	99	78	This work
HD 46375	NAR	Sep 08	18	M	3.2	–	–	Gaulme et al. (2010)
HD 73256	ESP	Jan 08	9	M	2.7	80	4	This work
HD 102195	ESP	Jan 08	10	M	12.4	44	25	This work
HD 130322	ESP	Jan 08	9	Y–M	2.5	84	58	This work
HAT-P-2	ESP	Jan 08	4	N	<40	75	–	This work
HD 179949	ESP	Jun 07	19	M	2.6	80	55	Fares et al. (2012)
HD 179949	ESP	Sep 09	10	M	3.7	90	36	Fares et al. (2012)
HD 189733	ESP	Jun 06	19	M	33	77	56	Moutou et al. (2007)
HD 189733	NAR	Jun 07	20	M	22	43	26	Fares et al. (2010)
HD 189733	NAR	Jul 08	24	M	36	33	17	Fares et al. (2010)
CoRoT-7	NAR	Jan 10	4	N	<150	100	–	This work
τ Bootis	ESP	Jun 06	12	M	1.8	–	–	Catala et al. (2007)
τ Bootis	NAR/ESP	Jun 07	2/30	M	3.7	83	60	Donati et al. (2008)
τ Bootis	ESP	Jan 08	40	M	3.1	38	20	Fares et al. (2009)
τ Bootis	NAR	Jun 08	9	M	2.3	87	36	Fares et al. (2009)
τ Bootis	NAR	Jul 08	19	M	1.7	91	62	Fares et al. (2009)
τ Bootis	NAR	Jun 09	16	M	2.7	88	43	This work
τ Bootis	NAR	Jan 10	10	M	3.8	62	46	This work
τ Bootis	NAR	Jan 11	18	M	3.2	70	37	This work
XO-3	ESP	Jan 08	15	N	<20	90	–	This work

3.6-m Canada–France–Hawaii Telescope (CFHT) on Mauna Kea or NARVAL at the 2-m Télescope Bernard Lyot (TBL) in Pic du Midi (France). Both instruments are twin high-resolution spectropolarimeters that measure the circular polarization in stellar spectral lines using multiple exposures. The spectral resolution and range are, respectively, 65 000 and 370–1000 nm in the polarization mode. Four exposures per observation are necessary to derive the circular polarization (Stokes V) profiles and check its significance with respect to spurious polarization signals. The data were collected between 2006 June and 2011 January, over a sample of 10 planet-host stars. For some stars of our sample, the number of collected spectra is limited, as they correspond to a first-investigation survey for spectropolarimetric detections in preparation for more intensive follow-up observations of detected fields. Table 1 gives a summary of the observations performed in this programme.

The data were reduced with the software LIBRE-ESPRIT that automatically extracts and calibrates intensity and polarization spectra. The least-square deconvolution (LSD; Donati et al. 1997) profiles are calculated to significantly improve the signal-to-noise ratio (SNR), using a mask adapted to the spectral type of each target. On average, more than 6000 stellar lines are used to produce these intensity and polarization profiles. The LSD profiles are corrected for the radial-velocity shift of the star, including the motion due to the planet. The radial-velocity precision of the stellar intensity profiles are better than 30 m s^{-1}.

3 STELLAR PROPERTIES

The stellar sample selected for our study includes 10 stars brighter than $V = 12$, hosting planets at orbital periods less than 11 d. Most of these planets are giant planets with masses larger than 0.22 $M_{\rm Jup}$, except CoRoT-7 b which is a telluric planet in an extremely short orbit (0.015 $M_{\rm Jup}$ and 0.85 d period; Léger et al. 2009). The stellar parameters adopted in this work are summarized in Table 2. The rotation periods are a critical parameter and often the least constrained one. The targets were originally selected for their short rotational periods, in order to allow observations with the two-week runs with ESPaDOnS; this does not apply, however, for HD 46375 and CoRoT-7, which were selected because of existing data of the *CoRoT* satellite (despite their long rotational periods). Note also that the rotation period of HD 130322 was recently updated to 26 d (Simpson et al. 2010), while it was given as 12 d in the planet discovery paper (Udry et al. 2000). There is also contradiction in the literature about the rotation period of HD 102195 (12 d in Ge et al. 2006 and 20 d in Melo et al. 2007): in our analysis, we choose the 12-d value which is based on photometric observations rather than on activity calibrations.

Concerning the stellar inclination, we use in general the value derived from the chosen rotation period, with $\sin i = v \sin i \times P_{\rm rot}/(2\pi R_\star)$. The reconstruction of the stellar magnetic field is, however, not very sensitive to a precise knowledge of the inclination (up to 20°; Morin et al. 2008).

4 SPECTROPOLARIMETRIC ANALYSES

When a sufficient number of detected Stokes V profiles is available, we reconstruct the best-fitting magnetic topology using a tomographic technique called Zeeman–Doppler imaging (ZDI) as developed by Donati et al. (1997, 2006) and described in these papers. ZDI consists of inverting series of Stokes V profiles into the stellar magnetic field topology responsible for producing these profiles. The problem is ill-posed, ZDI uses the principles of maximum entropy to retrieve the simplest image compatible with the data. The magnetic field is described by its radial, azimuthal and meridional components, all expressed in terms of spherical harmonics expansions. This description of the field allows us to calculate easily the contribution of each spherical harmonic order to the field, as well as the contribution of the poloidal and toroidal components and the

Table 2. Fundamental parameters of stars used in this work and some properties of their planets. The columns list the name of the star, its visual magnitude, spectral type, effective temperature, log of the gravity at the surface, [Fe/H], stellar mass, stellar radius, $v \sin i$, rotation period, orbital period of the planet, semimajor axis of the planetary orbit, planet's projected mass and the references.

Name	V (mag)	SpT	$T_{\rm eff}$ (K)	$\log g$	[Fe/H]	$M_\star$ ($M_\odot$)	$R_\star$ ($R_\odot$)	$v \sin i$ (km s^{-1})	$P_{\rm rot}$ (d)	$P_{\rm orb}$ (d)	a (au)	$M_{\rm p} \sin i$ $M_{\rm Jup}$	Ref.[a]
HD 46375	7.9	K1IV	5290	4.66	0.39	0.97	0.86	1.2	42	3.0236	0.0399	0.2272	G10, B06
HD 73256	8.08	G8	5636	4.30	0.26	1.05	0.89	3.2	14	2.5486	0.0371	1.869	B06, U03
HD 102195	8.05	K0V	5290	4.45	0.05	0.87	0.82	2.9	12.3	4.1138	0.0479	0.453	G06, M07
HD 130322	8.04	K0V	5330	4.41	−0.02	0.79	0.83	1.6	26.1	10.708	0.0896	1.043	U00, S10
HAT-P-2	8.71	F8	6290	4.22	0.12	1.36	1.64	20.8	3.8	5.6335	0.0687	9.09	P10
HD 179949	6.25	F8V	6168	4.34	0.14	1.21	1.19	7.0	7.6	3.0925	0.0439	0.902	B06, F12
HD 189733	7.7	K2V	5050	4.59	−0.03	0.82	0.76	2.97	12.5	2.2186	0.0310	1.140	B05, F10
CoRoT-7	11.7	G9V	5250	4.47	0.12	0.91	0.82	1.1	23.6	0.8536	0.0172	0.0151	B10
τ Bootis	4.5	F7V	6387	4.25	0.23	1.34	1.42	15.0	3.0	3.3124	0.0480	4.170	F09, B12
XO-3	9.8	F5V	6430	3.95	−0.18	1.41	2.08	18.3	3.7	3.1915	0.0454	11.79	JK08, W09

[a]G10: Gaulme et al. (2010), B06: Butler et al. (2006), U03: Udry et al. (2003), G06: Ge et al. (2006), M07: Melo et al. (2007), U00: Udry et al. (2000), S10: Simpson et al. (2010), P10: Pál et al. (2010), F12: Fares et al. (2012), B05: Bouchy et al. (2005), F10: Fares et al. (2010), B10: Bruntt et al. (2010), F09: Fares et al. (2009), B12: Brogi et al. (2012), JK08: Johns-Krull et al. (2008), W09: Winn et al. (2009).

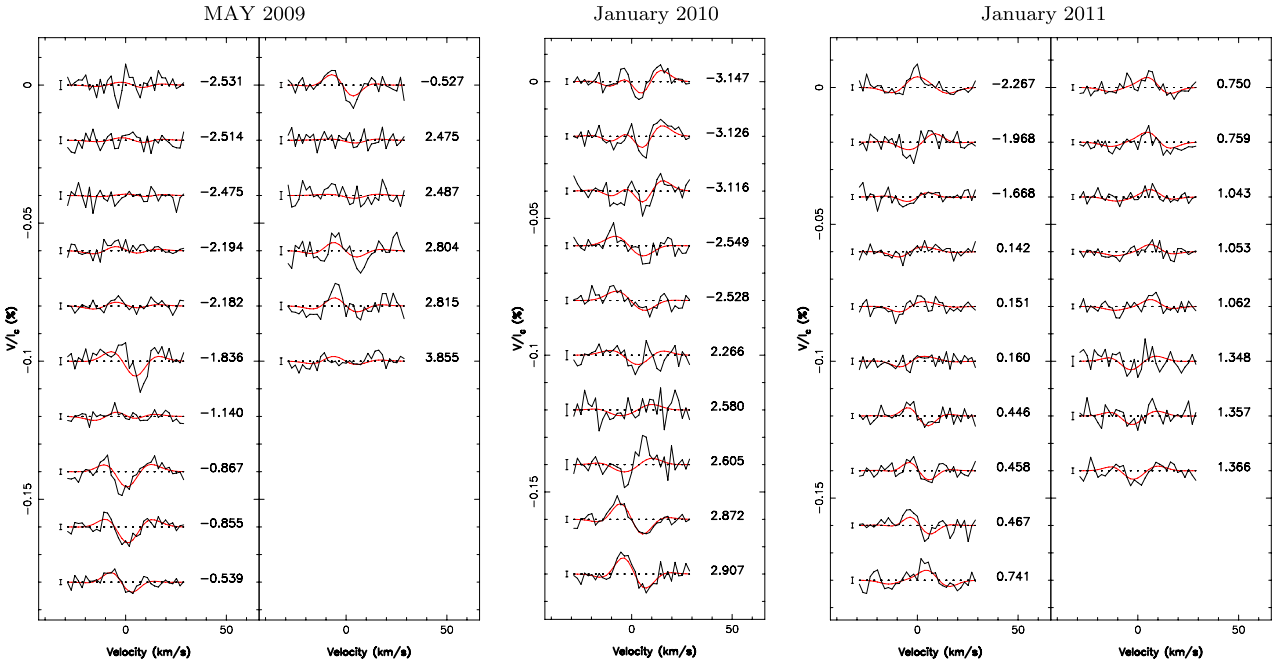

Figure 1. Circular polarization profiles of τ Boo obtained in 2009 May, 2010 January and 2011 January with TBL/NARVAL. The observed and synthetic profiles are shown in black and red, respectively. On the left of each profile we show a $\pm 1\sigma$ error bar, while on the right the rotational cycles are indicated.

degree of axisymmetry. Note that the axisymmetric contribution is given by modes with $m < l/2$.

4.1 The evolution of magnetic topology τ Boo

Previous spectropolarimetric analyses of five epochs of observations of τ Boo (F7V) have been described in Catala et al. (2007), Donati et al. (2008) and Fares et al. (2009). These data showed two occurrences of polarity reversals. The derived length of the magnetic cycle was about 2 yr; the temporal sampling of the observations, however, allowed other possible values for the cycle period.

New data were acquired with TBL/NARVAL during three separate epochs, in 2009 May (data spanning 19 d), 2010 January (20 d) and 2011 January (12 d). The journal of these new observations is shown in Appendix A (Table A1).

The LSD profiles were calculated using the same method and parameters as in Fares et al. (2009). We reconstructed the magnetic topology of τ Boo for all three epochs using the differential rotation (hereafter DR) measured by Fares et al. (2009). We used up to 8 degrees of spherical harmonics and an inclination of 45°. Our measurements of the inclination using ZDI in Catala et al. (2007), Donati et al. (2008) and Fares et al. (2009) agree with the measurements of Rodler et al. (2013) and Brogi et al. (2012) who used a different technique. We fit the V profiles to a level of reduced chi-square $\chi^2_{\rm r} = 0.95$. The observed and fitted profiles are shown in Fig. 1. The maps projected on a spherical coordinate system are shown in Fig. 2.

Previous observations have shown a large DR in τ Boo, with a surface shear of the order of $d\Omega = 0.4 \pm 0.1$ rad d^{-1} and an equatorial angular velocity of $\Omega_{\rm eq} = 2.0 \pm 0.1$ rad d^{-1} (Donati et al. 2008; Fares et al. 2009). DR is again detected in the 2009 May data

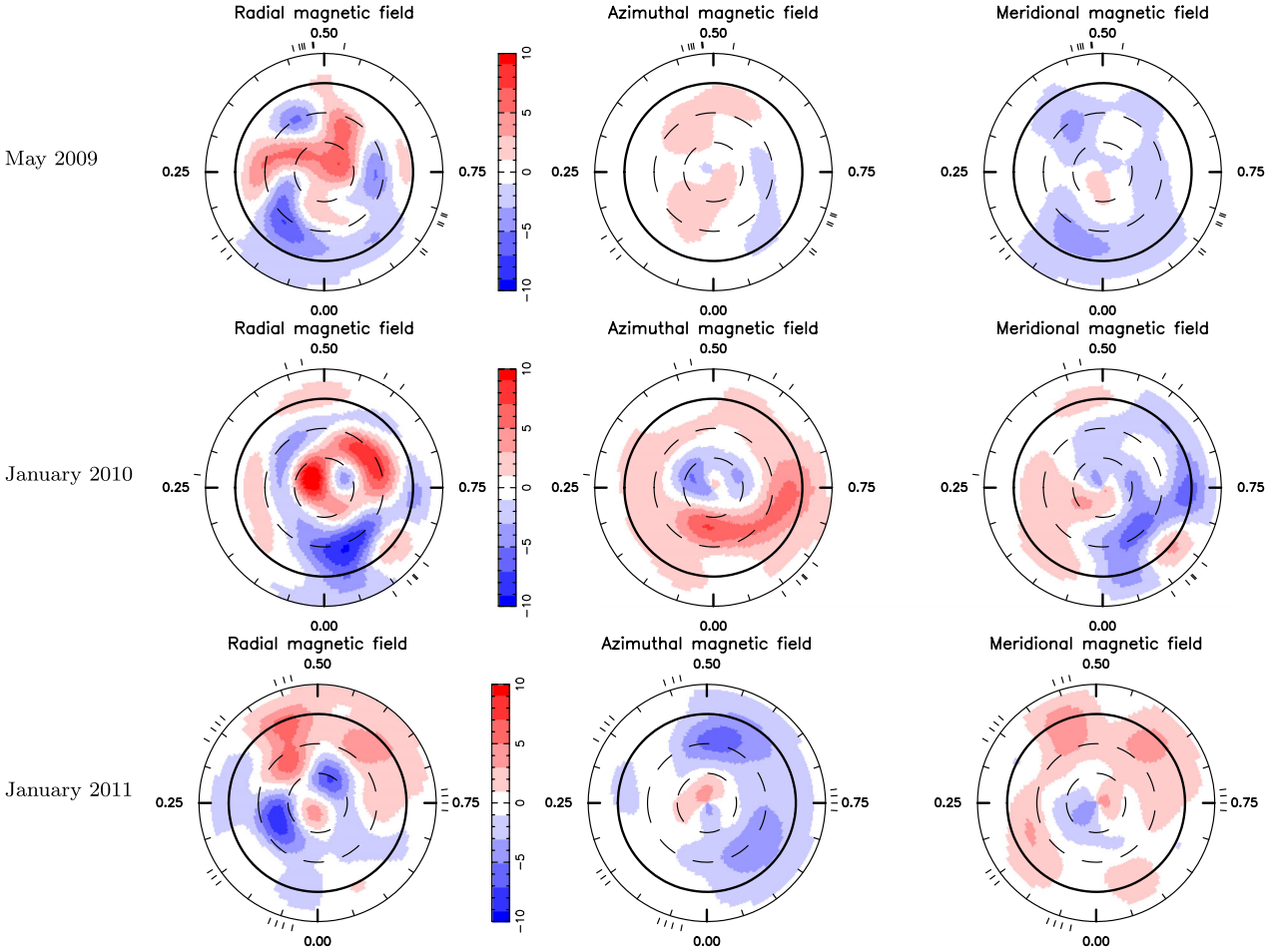

Figure 2. Magnetic topology of τ Boo reconstructed from profiles in Fig. 1: 2009 May (top row); 2010 January (middle row) and 2011 January (bottom row). The radial, azimuthal and meridional components of the field (with magnetic field strength labelled in G) are depicted. The star is shown in flattened polar projection down to latitudes of 30°, with the equator depicted as a bold circle and parallels as dashed circles. The radial ticks around each plot indicate rotational phases of observations.

set, with corresponding values of $\Omega_{\rm eq} = 1.98 \pm 0.01$ rad d^{-1}and $\mathrm{d}\Omega = 0.15 \pm 0.03$ rad d^{-1}. The value of $\mathrm{d}\Omega$ is significantly smaller than values measured in previous epochs. Although our observations cover 20 d, the rotational phases do not sample the stellar surface very widely, which may induce a bias in deriving the DR. For this reason, we reconstructed the maps using the DR parameters as measured in previous epochs, for all data.

The properties of the reconstructed magnetic maps for the three new epochs are summarized in Table 3. The average magnetic field ranges from 2.7 to 3.8 G, with values very similar to the ones reported in earlier analyses (1.7–3.7 G in Fares et al. 2009). The contribution of the toroidal component to the total magnetic energy varies from 12 to 30 per cent, in a smaller extent with respect to earlier epochs (9–62 per cent). The last epoch of observation, in 2011 January, shows a new polarity reversal compared to 2010 January. In addition, the field has also switched polarity between 2008 July (last map in Fares et al. 2009) and 2009 May. As observed earlier, the field configuration evolves inside a cycle: between 2009 May and 2010 January, the energy distributed in the radial field has decreased while the energy in the azimuthal field has increased.

Period of magnetic cycle

In order to determine the length of τ Boo's magnetic cycle, we performed a period search similar to the one described in Fares et al. (2009). We calculated the (signed) magnetic flux in both the radial and azimuthal components of the field for each reconstructed map. In the case of the radial field, the flux is counted positive for latitudes greater than 30° and negative for latitudes between 0° and 30°. We then simultaneously fitted the two fluxes with two sine waves of equal period, the period being varied on a range of 100–1300 d. We found, as in Fares et al. (2009), two periods that fit the data well. The first one is of 740 d (2 yr) and the second one is of 240 d (8 months), see Fig. 3. We then calculated the false-alarm probability (FAP) of these periods. We produced 10 000 data sets by night shuffling and fitted each data set following the same procedure described above. The FAP is the number of data sets for which the $\chi^2_{\rm r}$ is smaller than the $\chi^2_{\rm r}$ of our periods divided by 10 000. We find an FAP of 3 per cent for the 240 d period and an FAP of 15 per cent for the 740 d period.

4.2 HD 73256

Nine ESPaDOnS spectra of HD 73256 (G8) spanning 11 d were obtained in 2008 January. Six circular polarization signatures are detected. The adopted stellar inclination is 75° deduced from the rotational period measured by photometry (Udry et al. 2003). DR is not detected in the data and thus is fixed to zero for the reconstruction of the magnetic field. When correcting each LSD

Table 3. Summary of magnetic topology evolution of τ Boo: average magnetic field B, percentage of the toroidal energy relative to the total energy, percentage of the energy contained in the axisymmetric modes of the poloidal component (modes with $m < l/2$) and percentage of the energy contained in the modes of $l \leq 2$ of the poloidal component for each epoch of observations.

Epoch	B (G)	Per cent toroidal (per cent)	Per cent axisym in poloidal (per cent)	Per cent $l \leq 2$ in poloidal (per cent)	Reference
2007 June	3.7	17	60	52	Donati et al. (2008)
2008 January	3.1	62	20	50	Fares et al. (2009)
2008 June	2.3	13	36	36	Fares et al. (2009)
2008 July	1.7	9	62	47	Fares et al. (2009)
2009 May	2.7	12	43	47	This work
2010 January	3.8	38	46	40	This work
2011 January	3.2	30	37	50	This work

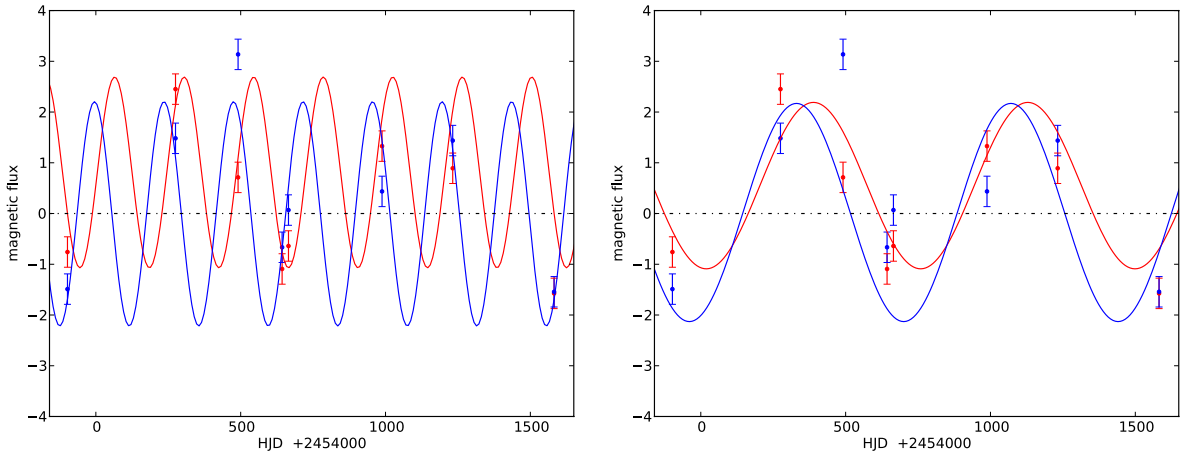

Figure 3. Fluxes of the radial field (red) and azimuthal field (blue) versus HJD, calculated for the Northern hemisphere of τ Boo. In the particular case of B_r, the magnetic flux is counted positive for latitudes superior to 30° and negative for latitudes between 0° and 30° to take into account the contribution of both dipolar and quadrupolar terms of the poloidal field (as in Fares et al. 2009). The best sinusoidal fit for $P = 240$ d (left-hand panel) and $P = 740$ d (right-hand panel) are plotted.

profile for the radial velocity of the star, we found that our measurements did not match the orbital ephemeris published in the literature, $T_0 = 2452\,500.18 \pm 0.28$ (Udry et al. 2003). We updated the orbit phase using a measured $T_0 = 2452\,500.42$. The magnetic map is reconstructed for a χ^2_r of 1.15, which produces a reasonable fit to the Stokes V profiles (Fig. 4 first column). The magnetic field that best matches the observations is an 80 per cent poloidal field with a mean strength of 2.7 G. A small fraction of the poloidal field is in axisymmetric modes (∼4 per cent). The reconstructed topology of the stellar surface field is shown in Fig. 5 (top row).

4.3 HD 102195

10 spectra of HD 102195 (K0V) were obtained with ESPaDOnS in 2008 January (spanning 11 d), among which eight show a definite detection of the magnetic field. The data do not show any evidence for DR, we consider a solid rotation at the 12 d period measured by Ge et al. (2006) and an inclination of 50° for the magnetic field reconstruction. The radial velocity of the star is corrected from the systemic velocity and the planet induced motion, as given in the literature (Melo et al. 2007). Our ESPaDOnS observations are not of sufficient velocity precision to permit the detection of the planet signal, especially on this star that exhibits activity jitter (Melo et al. 2007).

Our observations cover almost one stellar rotation. The circular polarization profiles are well fitted as shown in Fig. 4 (second column). The field modelling is achieved for $\chi^2_r = 1.2$. The characteristics of the best-fitting magnetic model features a dipole contributing by 70 per cent to the poloidal component. The field's mean strength is of 12.5 G, 45 per cent of the magnetic energy in the poloidal field (Fig. 5, second row) and 25 per cent of the poloidal field is axisymmetric.

4.4 HD 46375

HD 46375 (K1IV) has been first observed with ESPaDOnS in 2008 January and then with NARVAL in 2008 October. This later data set has been obtained simultaneously with *CoRoT* photometric observations and is described in Gaulme et al. (2010). We describe in the following the data obtained with ESPaDOnS, although its temporal coverage is much poorer: only one quarter of the rotational period has been covered. Such a poor sampling of the stellar surface prevents the reconstruction of a magnetic map. We just recall the properties of the field as characterized by the NARVAL observations in 2008 October: the field is dominated by a slightly tilted and mostly axisymmetric dipole with respect to the rotation axis; the magnetic strength at the pole is of the order of 5 G. The Stokes V profiles observed in 2008 January with ESPaDOnS (Fig. 4, third column) are compatible with a dipole observed partially and also correspond to a dipole of a few G amplitude. We cannot however constrain the dipole tilt nor get a high confidence on the mean magnetic strength of the large-scale structure. The map given in

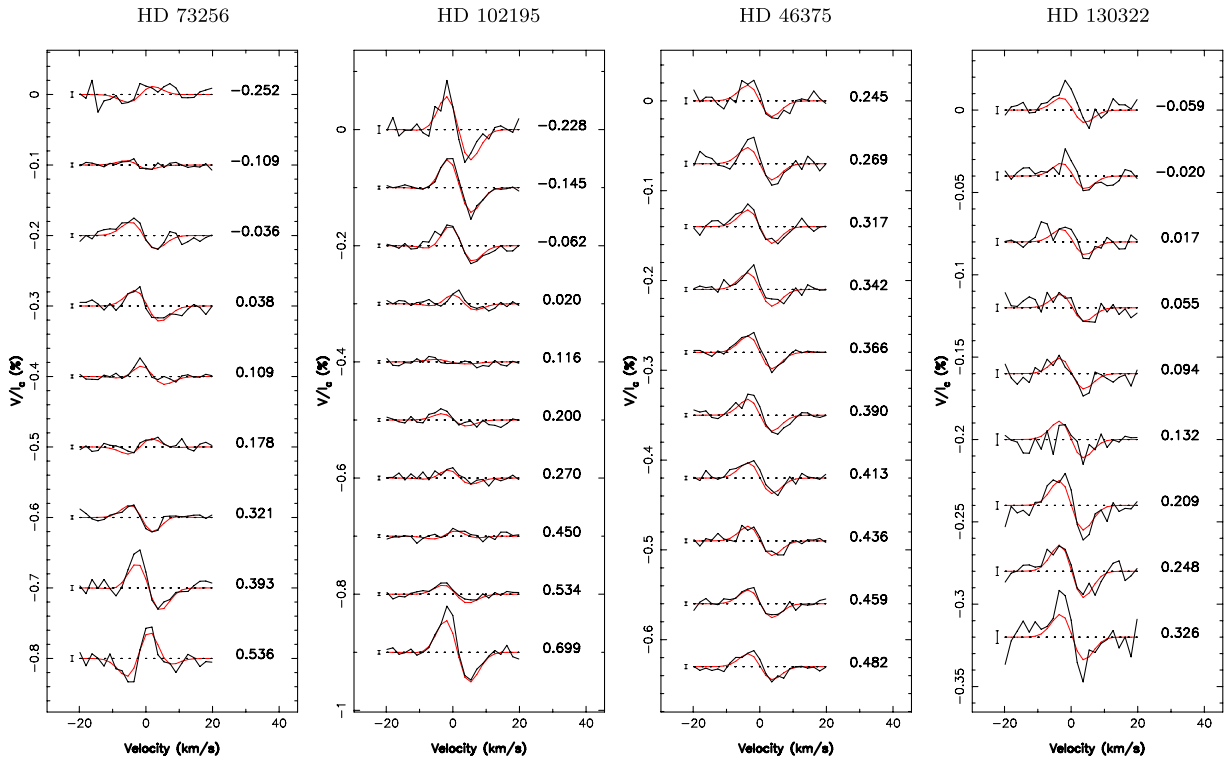

Figure 4. Circular polarization profiles obtained in 2008 January with CFHT/ESPaDOnS for stars HD 73256, HD 102195, HD 46375 and HD 130322, respectively, from left to right. See legend details in Fig. 1.

Fig. 5 (third row) is indicative and fairly similar to the one obtained by Gaulme et al. (2010).

4.5 HD 130322

Nine ESPaDOnS spectra of HD 130322 (K0V) were secured in 2008 January. The rotation period of this star is 26 d (Simpson et al. 2010), much longer than our observing run of 10 d. As a consequence, only one third of the stellar surface is observed. This makes difficult a full reconstruction of the magnetic topology, since we do not have observational constraints on the unobserved part of the star (see appendix B in Fares et al. 2012). The circular polarization profiles are, however, significantly detected in all observing epochs.

We adopt a value of 80° for the stellar inclination and reconstruct the map with a χ^2_r of 0.9 (Fig. 5, fourth row). The circular polarization profiles (Fig. 4, fourth column) are well fitted by a magnetic structure dominated by a dipole (only ∼16 per cent of the field energy is toroidal) of 2.5 G mean strength. Data over more than a full rotation period would be needed to confirm this result and could still reveal a more complex large-scale structure of the magnetic field.

4.6 HD 189733

Table 1 includes three observational campaigns of HD 189733 (K2V) using ESPaDOnS and NARVAL in 2006, 2007 and 2008 for completion with respect to the target sample presented here. However, their analysis has already been published in Moutou et al. (2007) and Fares et al. (2010) and will not be repeated here. HD 189733 has a mainly toroidal surface magnetic field with a strength of 20–40 G. The stellar surface has a DR of $d\Omega = 0.146 \pm 0.049$ rad d^{-1}. The field extrapolation up to the location of the planet has been derived by Fares et al. (2009) and Cohen et al. (2011). The planet is found to cross different stellar field configurations along its orbit. This makes the reconnection events between stellar and planetary magnetic fields possible on fractions of the orbit. The planetary radio emission from magnetospheric interaction with the stellar wind varies along the orbit (Fares et al. 2010)

4.7 HD 179949

Two epochs of ESPaDOnS observations of HD 179949 (F8V) have been discussed in Fares et al. (2012). The 2009 data set is part of a joined campaign with *XMM* and ground-based spectroscopic data taken simultaneously with the spectropolarimetric observations. The additional data are described in Scandariato et al. (2013). HD 179949 exhibits a weak and mainly poloidal magnetic field of a few G and a tilt of ∼70°. A DR of $d\Omega = 0.216 \pm 0.061$ rad d^{-1} has been measured. In this case also, the field at the stellar surface has been extrapolated up to the planetary orbit, for further studies concerning modelling the interactions (Fares et al. 2012).

4.8 Stars without detected fields

4.8.1 XO-3

We have secured 20 independent observations of XO-3 (F5V) with ESPADONS in 2009 October. Despite a high SNR for most spectra (12 out of 20 have SNR above ∼300), there was no detection of polarization in the Stokes *V* profiles.

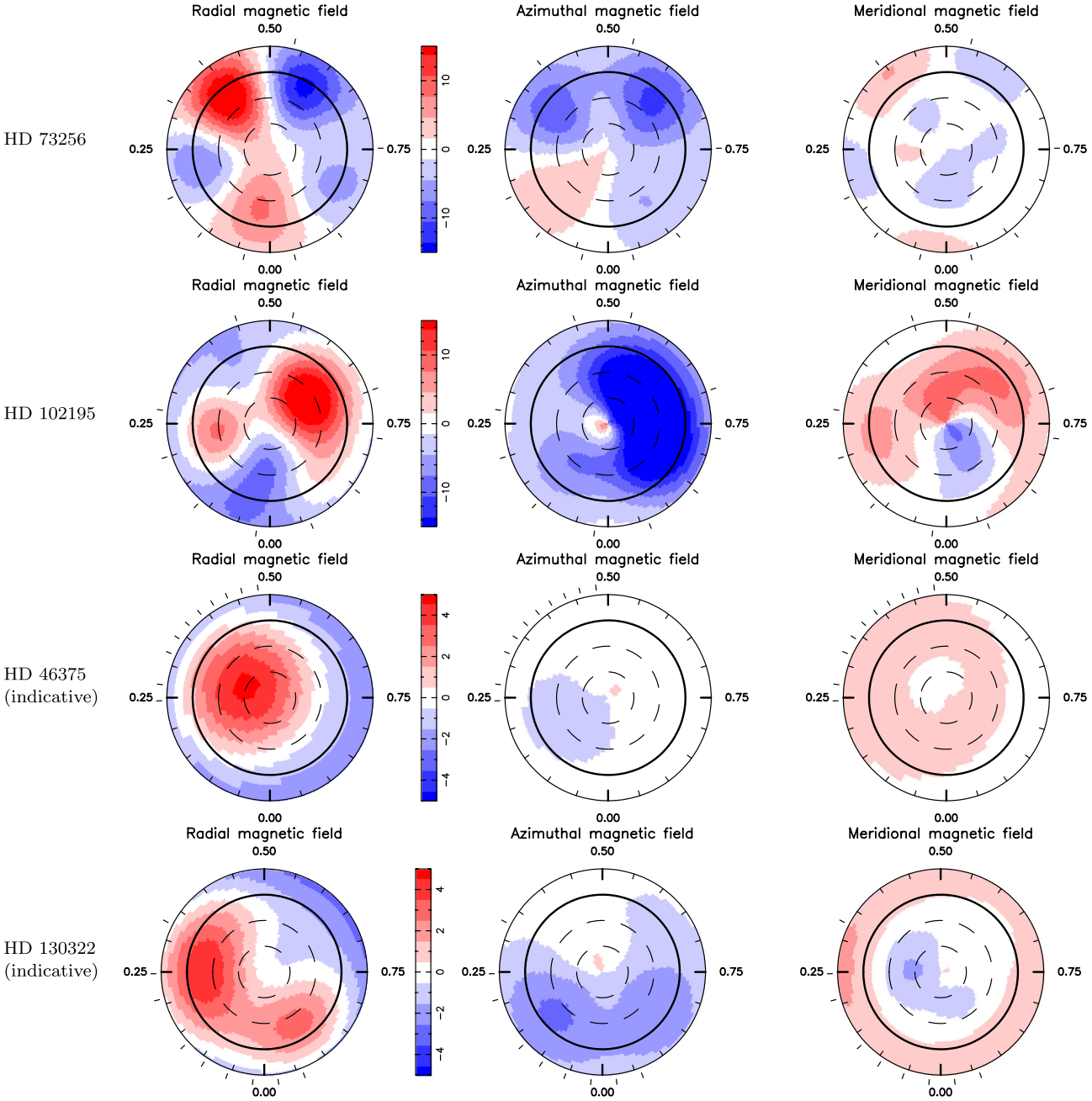

Figure 5. Magnetic maps of HD 73256, HD 102195, HD 46375 and HD 130322 from top to bottom rows. See legend details in Fig. 5.

In order to quantify an upper limit for a magnetic field of XO-3, we propose the following analysis.

(i) We select a star with similar mass and a rotation period to XO-3, but for which we have a magnetic field detection. The reconstructed magnetic field of the chosen star is used as a magnetic topology model for X0-3.

(ii) From this fake magnetic field, we calculate Stokes *V* profiles. We compare these profiles to the observed noise properties at the phases of our observations.

(iii) If the signal exceeds the noise and should have led to a detection, we decrease the field strength, without changing its topology. We repeat (ii) until the signal from the fake Stokes *V* profile is just about the noise level of the observations, at which a lower limit on the magnetic field of the star is derived.

This analysis may give a reasonable order of magnitude of the maximum field strength excluded by our data for a chosen field topology. It must be noted, however, that other parameters may alter this value as the inclination (low impact), the temporal sampling of the observations and the field complexity. This attempt to quantify our non-detection should therefore not be overinterpreted.

In the case of XO-3 where we have numerous observations and a fast rotating star ($v \sin i = 18.3$ km s^{-1}), the detection limit has the most relevant significance. We injected signals corresponding to two stars where a magnetic topology has been deduced from previous observations, and relatively close in stellar properties to

XO-3: HD 102195 (Section 4.3) and HD 179949 (Fares et al. 2012). HD 179949 has an effective temperature close to that of XO-3, but has Rossby number >1.0, while HD 102195 has a lower mass than XO-3, but has, as XO-3, Rossby number <1.0 (magnetic fields show similar properties for stars in different Rossby regimes, see Section 5). A field with similar properties than HD 102195 (with mean field strength ∼10 G) projected on the observation space of XO-3 remains undetected at 3σ except in one spectrum and represents a reasonable detection limit in the context of an HD 102195's 55 per cent toroidal magnetic field topology. The field of HD 179949, as characterized from the 2009 ESPaDOnS campaign (Fares et al. 2012), is undetectable in the signal of XO-3. We multiplied by 10 all components of this magnetic field and found that the fake Stokes *V* signatures would have been detected in 7 over the 15 best quality spectra with a significance larger than 3σ. Thus, a mostly (90 per cent) poloidal field with an amplitude of 20 G would have been unambiguously detected. We adopt this more conservative value for an upper limit for the magnetic field strength of XO-3 during the 2009 observation campaign.

4.8.2 HAT-P-2 = HD 147506

HAT-P-2 (F8) has been observed four times between 2007 June 26 and July 1. None of the spectra shows a detection of the magnetic field, with a mean rms noise level in the LSD profiles of 0.5×10^{-4}. HAT-P-2 is a fast rotating star with an effective temperature of 6290 K, so its properties closely match the ones of τ Boo. In order to investigate the detection limit of the magnetic field in our data, we thus used one of the magnetic configurations depicted for τ Boo, scaled the field strength and calculated the fake Stokes *V* signatures that would have been produced at our observing sampling. We find that a 75 per cent poloidal field of 40 G would have been detected in two over the four observed phases. The actual field is thus either of very different configuration or of lower strength (or both).

4.8.3 CoRoT-7

Four spectra of CoRoT-7 (G9V) have been secured with NARVAL in 2010 January. Due to the faint luminosity of the star (*V* magnitude = 11.7), the field detection represents a real challenge, especially for NARVAL. The SNR of the profiles is 10 times lower than that for HAT-P-2. In all four spectra, there is a spurious detection in the Stokes *V* profile, also detected in the null-polarization check profiles. Only the last exposure shows a marginal detection of the magnetic field, with a Stokes *V* profile slightly larger than the null profile. We applied the same strategy described for XO-3 and HAT-P-2, taking a dipole as the magnetic model for this star (similar to the topology of HD 46375). We compared the fake Stokes *V* signatures that a dipolar field would produce at our observing phases. We find that a dipole with more than 150 G strength would have been significantly detected in two spectra over the four available ones and beyond the marginal detection on 2008 January 27. The detection limit represents a poorer constraint than for XO-3 and HAT-P-2, because the star is of lower mass, a slower rotator, and the spectra have lower SNR.

5 DISCUSSION AND SUMMARY

A summary of the main characteristics of the stellar magnetic fields observed in this study is given in Table 1. When the field is not detected, the upper value derived as explained above is shown. The stars of this study, with stellar masses 0.8–1.4 $M_\odot$, feature large-scale magnetic fields of 2–40 G. Except at two epochs for HD 189733 and HD 102195, all other targets have mainly poloidal fields, with varying degrees of axisymmetry.

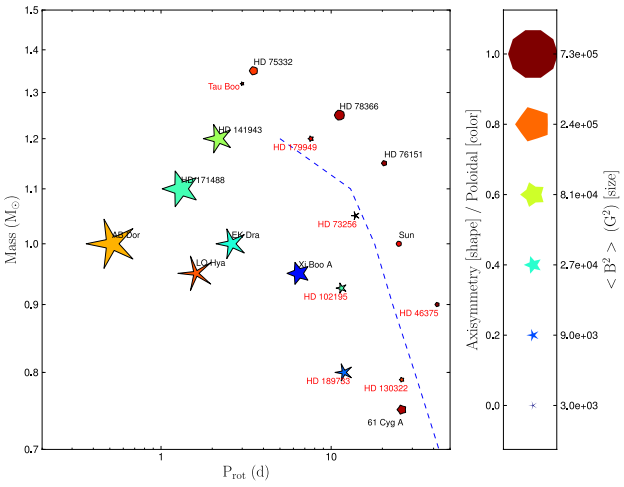

Figure 6. Mass–rotation diagram of 18 reconstructed stellar magnetic fields (not including dM stars for instance). Planet-host stars studied in this paper have their names indicated in red, while other stars without detected HJ have their names indicated in black (data from Donati & Landstreet 2009). The dashed line represents Rossby number = 1.0 (calculated using results of Landin, Mendes & Vaz 2010). The size of the symbol represents the field strength, its colour the contribution of the poloidal component to the field and its shape how axisymmetric the poloidal component is. For τ Boo, we show here the field for one epoch of observation (mainly poloidal). HJ host stars do not seem to have different magnetic properties than the other stars.

The presence of a giant planet at a small orbital distance is thought to have influences on the star. Empirical evidence suggest that tidal interactions can cause excess rotation of the parent star (Pont 2009). Cuntz, Saar & Musielak (2000) suggest that these interactions can cause local instabilities in the tidal bulges and thus modify the local dynamo on action in these regions. Cebron et al. (2011a,b) present theoretical work on the effect of tidally driven elliptical instability on a star hosting a hot-Jupiter (HJ) and suggest that eventually these instabilities can produce a dynamo. In order to study possible peculiarities in the magnetic topologies of HJ host stars, one should compare their magnetic topologies to that of similar stars without detected close-in giant planets. Fig. 6 shows a mass–rotation plane including the magnetic properties of the stars of our sample (whose names are shown in red) as well as other published stellar field properties (from Donati & Landstreet 2009). A main transition appears in this plot for stars with masses above 0.5 $M_\odot$: (i) below Rossby number of ∼1, the large-scale field is mainly toroidal, with a non-axisymmetric poloidal component and (ii) above Rossby number of ∼1, the field is weaker, poloidal and axisymmetric. The long-term evolution of the magnetic fields should however be taken into account, with possible cycles, as for the Sun and a few other known examples (Donati et al. 2008; Fares et al. 2009; Morgenthaler et al. 2011). Our HJ host stars show similar field topologies as the stars without a discovered close-in giant planet. The strength of their magnetic fields seems weaker; however, our sample is basically of stars chosen for radial-velocity studies, they are less active than the other stars shown in Fig. 6. In addition, if the data quality is poor (poor SNR and poor phase coverage), the reconstructed magnetic field strength is reduced below what would be reconstructed with higher quality data (see Fares et al. 2012). In order to comment of the field strength of planet-host stars, it is necessary to enlarge our sample.

τ Boo's magnetic cycle is confirmed to be a short one. Observed between 2006 June and 2011 January, the large-scale magnetic field of this star switches polarity yearly. However, the cycle duration might be of 2 yr or of 8 months, as both periods are good solutions for the data we have. In the frequency domain, the 240 d period is the third harmonic of the 740 d period. The period of 740 d seems more likely. Previous studies of the chromospheric activity of this star found a period of 126 d persistent over 30 yr (Baliunas et al. 1997; Maulik, Donahue & Baliunas 1997). If the relation between the activity cycle to the large-scale magnetic field cycle in stars is similar to that of the Sun, this favours the 8 month period for the magnetic cycle. However, such a relation is not known for stars (there is a lack of observed large-scale magnetic cycles), and thus it cannot help us rule out one of the two values we get. In order to favour one value over the other, we suggest dense observations of this star over a year, with at least four epochs of observations. Constraining the period will permit a comparison with the solar chromospheric/magnetic cycle behaviour.

Poppenhaeger, Günther & Schmitt (2012) observed τ Boo in X-rays over six epochs (one observation in 2003 June and then five between 2010 June and 2011 June). The star shows variability in X-rays, but a cyclic behaviour was not observed. They conjecture that the lack of X-ray cycles could be explained by their sparse sampling or that the polarity switch could be an artificial feature from the reconstruction method (ZDI) rather than being a real polarity switch. We note however that the lack of X-ray cycle does not rule out the presence of polarity switches (magnetic cycles), as have been predicted by theoretical works (McIvor et al. 2006, see also Baumann et al. 2004; Işık, Schmitt & Schüssler 2011). Furthermore, in the particular case of τ Boo, Vidotto et al. (2012) simulated its stellar wind through the magnetic cycle and studied mass-loss and angular-momentum loss rates, as well as X-ray emission measure and planetary radio emission. In their study, they used the magnetic maps from Fares et al. (2009), Donati et al. (2008) and Catala et al. (2007) as a boundary condition for the stellar magnetic field (they thus considered the polarity switch in their model). They find that the emission measure does not vary during the cycle, suggesting that the quiescent X-ray emission of τ Boo does not change significantly over the cycle, agreeing with the findings of Poppenhaeger et al. (2012).

The goal of this work is to study for the first time the magnetic fields of a sample of planet-host stars. When possible, we reconstructed the stellar magnetic fields. We found a wide range of topologies. In order to check if these topologies are peculiar, we compared them to those of stars without detected HJ. We found that these planet-host stars do not show peculiar magnetic behaviours. Our study shows that the stellar magnetic field topology is usually more complex than a simple dipole or quadrupole. Thus, it is essential to use the reconstructed maps in simulations (instead of modelling the field by a simple dipole). Our work is thus a basis for future star–planet interactions simulations, wind models, and simulations of radio and X-ray emission. We will make our magnetic maps available to the public on the following link http://lamwws.oamp.fr/exo/starplanetinteractions/mtphs.

ACKNOWLEDGEMENTS

RF acknowledges support from STFC consolidated grant ST/J001651/1. This work is based on observations obtained with ESPaDOnS at the CFHT and with NARVAL at the TBL. CFHT/ESPaDOnS are operated by the National Research Council of Canada, the Institut National des Sciences de l'Univers of the Centre National de la Recherche Scientifique (INSU/CNRS) of France and the University of Hawaii, while TBL/NARVAL are operated by INSU/CNRS. We thank the CFHT and TBL staff for their help during the observations. We thank an anonymous referee for their comments.

REFERENCES

Baliunas S. L., Henry G. W., Donahue R. A., Fekel F. C., Soon W. H., 1997, ApJ, 474, L119
Baumann I., Schmitt D., Schüssler M., Solanki S. K., 2004, A&A, 426, 1075
Bouchy F. et al., 2005, A&A, 444, L15
Brogi M., Snellen I. A. G., de Kok R. J., Albrecht S., Birkby J., de Mooij E. J. W., 2012, Nat, 486, 502
Bruntt H. et al., 2010, A&A, 519, A51
Butler R. P. et al., 2006, ApJ, 646, 505
Catala C., Donati J.-F., Shkolnik E., Bohlender D., Alecian E., 2007, MNRAS, 374, L42
Cebron D., Le Bars M., Moutou C., Maubert P., Le Gal P., 2011a, EPSC-DPS Joint Meeting 2011, Tides Induced Magnetic Field in the Solar System. p. 1080, available at: http://meetings.copernicus.org/epsc-dps2011
Cebron D., Moutou C., Le Bars M., Le Gal P., Farès R., 2011b, in Bouchy F., Díaz R., Moutou C., eds, European Physical Journal Web of Conferences, Vol. 11, Tidal Instability in Exoplanetary Systems Evolution. p. 3003, available at: http://dx.doi.org/10.1051/epjconf/20101103003
Cohen O., Drake J. J., Kashyap V. L., Sokolov I. V., Gombosi T. I., 2010, ApJ, 723, L64
Cohen O., Kashyap V. L., Drake J. J., Sokolov I. V., Garraffo C., Gombosi T. I., 2011, ApJ, 733, 67
Cranmer S. R., Saar S. H., 2007, preprint (astro-ph/0702530)
Cuntz M., Saar S. H., Musielak Z. E., 2000, ApJ, 533, L151
Dobbs-Dixon I., Lin D. N. C., Mardling R. A., 2004, ApJ, 610, 464
Donati J.-F., Landstreet J. D., 2009, ARA&A, 47, 333
Donati J.-F., Semel M., Carter B. D., Rees D. E., Collier Cameron A., 1997, MNRAS, 291, 658
Donati J.-F. et al., 2006, MNRAS, 370, 629
Donati J.-F. et al., 2008, MNRAS, 385, 1179
Fares R. et al., 2009, MNRAS, 398, 1383
Fares R. et al., 2010, MNRAS, 406, 409
Fares R. et al., 2012, MNRAS, 423, 1006
Gaulme P. et al., 2010, A&A, 524, A47
Ge J., van Eyken J., Mahadevan S., DeWitt C., Kane S. R., Cohen R., 2006, ApJ, 648, 683
Işık E., Schmitt D., Schüssler M., 2011, A&A, 528, A135
Jardine M., Collier Cameron A., Donati J.-F., 2002, MNRAS, 333, 339
Johns-Krull C. M. et al., 2008, ApJ, 677, 657
Lai D., Foucart F., Lin D. N. C., 2011, MNRAS, 412, 2790
Landin N. R., Mendes L. T. S., Vaz L. P. R., 2010, A&A, 510, A46
Lanza A. F., 2012, A&A, 544, A23
Léger A. et al., 2009, A&A, 506, 287
Maulik D., Donahue R. A., Baliunas S. L., 1997, Technical Report, Persistent Sub-Yearly Chromospheric Variations in Lower Main-Sequence Stars: Tau Booe and alpha COM. Harvard-Smithsonian Center for Astrophysics, Cambridge
McIvor T., Jardine M., Mackay D., Holzwarth V., 2006, MNRAS, 367, 592
Melo C. et al., 2007, A&A, 467, 721
Morgenthaler A., Petit P., Morin J., Aurière M., Dintrans B., Konstantinova-Antova R., Marsden S., 2011, Astron. Nachr., 332, 866
Morin J. et al., 2008, MNRAS, 390, 567
Moutou C. et al., 2007, A&A, 473, 651
Pagano I., Lanza A. F., Leto G., Messina S., Barge P., Baglin A., 2009, Earth Moon Planets, 105, 373
Pál A. et al., 2010, MNRAS, 401, 2665
Pont F., 2009, MNRAS, 396, 1789
Poppenhaeger K., Günther H. M., Schmitt J. H. M. M., 2012, Astron. Nachr., 333, 26

Rodler F., Kürster M., López-Morales M., Ribas I., 2013, Astron. Nachr., 334, 188
Scandariato G. et al., 2013, A&A, 552, A7
Shkolnik E., Walker G., Bohlender D., 2003, ApJ, 597, 1092
Shkolnik E., Walker G., Bohlender D., Gu P., Kürster M., 2005, ApJ, 622, 1075
Shkolnik E., Bohlender D. A., Walker G. A. H., Collier Cameron A., 2008, ApJ, 676, 628
Simpson E. K., Baliunas S. L., Henry G. W., Watson C. A., 2010, MNRAS, 408, 1666
Udry S. et al., 2000, A&A, 356, 590
Udry S. et al., 2003, A&A, 407, 679
Vidotto A. A., Fares R., Jardine M., Donati J.-F., Opher M., Moutou C., Catala C., Gombosi T. I., 2012, MNRAS, 423, 3285
Walker G. A. H. et al., 2008, A&A, 482, 691
Winn J. N. et al., 2009, ApJ, 700, 302

APPENDIX A: JOURNAL OF OBSERVATIONS

In this appendix, the detailed journal of observations (Tables A1, A2 and A3) is given for all data of the survey, except the ones already published in Catala et al. (2007), Donati et al. (2008), Moutou et al. (2007), Fares et al. (2009), Fares et al. (2010) and Fares et al. (2012).

Table A1. Journal of observations of τ Boo. Columns 1–12 sequentially list the star name, UT date, instrument used, the heliocentric Julian date (at mid-exposure), the UT time (at mid-exposure), the complete exposure time, the peak signal-to-noise ratio (SNR) (per 2.6 km s^{-1} velocity bin) of each observation (around 700 nm), the rotational cycle, the radial velocity (RV) associated with each exposure, the rms noise level (relative to the unpolarized continuum level I_c and per 1.8 km s^{-1} velocity bin) in the circular polarization profile produced by LSD, the longitudinal magnetic field and the FAP of the detection of the magnetic signature.

Star	Date	Instrument	HJD (245 4000+)	UT (h:m:s)	T_{exp} (s)	SNR	ϕ_{rot}	RV (km s^{-1})	σ_{LSD} ($10^{-4} I_c$)	B_l (G)	FAP
τ Boo	27-May-09	Narval	979.391 42	21:18:08	4 × 700	1030	−2.531	−16.163	0.33	−0.0 ± 1.5	3.279×10^{-01}
τ Boo	27-May-09	Narval	979.440 73	22:29:08	4 × 700	1410	−2.514	−16.189	0.25	−0.7 ± 1.1	5.612×10^{-01}
τ Boo	27-May-09	Narval	979.559 91	01:20:46	4 × 600	1430	−2.475	−16.276	0.27	0.2 ± 1.2	8.699×10^{-01}
τ Boo	28-May-09	Narval	980.402 58	21:34:17	4 × 700	1650	−2.194	−16.821	0.22	−0.4 ± 1.0	6.172×10^{-01}
τ Boo	28-May-09	Narval	980.438 25	22:25:39	4 × 700	1710	−2.182	−16.832	0.22	−0.6 ± 1.0	9.594×10^{-01}
τ Boo	29-May-09	Narval	981.476 84	23:21:18	4 × 700	1500	−1.836	−16.278	0.26	1.0 ± 1.2	5.935×10^{-07}
τ Boo	31-May-09	Narval	983.563 41	01:26:07	4 × 700	1880	−1.140	−16.813	0.19	0.4 ± 0.9	8.525×10^{-01}
τ Boo	01-Jun-09	Narval	984.383 96	21:07:46	4 × 700	1880	−0.867	−16.643	0.19	−1.8 ± 0.8	2.259×10^{-11}
τ Boo	01-Jun-09	Narval	984.418 75	21:57:52	4 × 700	1830	−0.855	−16.620	0.19	−0.8 ± 0.9	5.689×10^{-06}
τ Boo	02-Jun-09	Narval	985.366 61	20:42:52	4 × 700	1800	−0.539	−15.948	0.19	0.8 ± 0.8	7.379×10^{-02}
τ Boo	02-Jun-09	Narval	985.401 38	21:32:56	4 × 700	1880	−0.527	−15.951	0.19	1.6 ± 0.8	1.343×10^{-08}
τ Boo	11-Jun-09	Narval	994.409 98	21:46:06	4 × 700	1380	2.475	−16.520	0.26	1.2 ± 1.2	6.621×10^{-01}
τ Boo	11-Jun-09	Narval	994.444 75	22:36:11	4 × 700	1380	2.487	−16.484	0.28	1.4 ± 1.3	4.310×10^{-01}
τ Boo	12-Jun-09	Narval	995.395 00	21:24:37	4 × 700	1360	2.804	−15.935	0.30	−1.7 ± 1.3	2.871×10^{-02}
τ Boo	12-Jun-09	Narval	995.429 78	22:14:42	4 × 700	1480	2.815	−15.923	0.28	−1.9 ± 1.2	8.053×10^{-03}
τ Boo	15-Jun-09	Narval	998.549 78	01:07:48	4 × 600	1690	3.855	−15.940	0.24	−2.3 ± 1.1	8.522×10^{-01}
τ Boo	25-Jan-10	Narval	1222.664 29	03:55:40	4 × 600	1730	−3.147	−16.860	0.20	−1.2 ± 0.9	8.225×10^{-07}
τ Boo	25-Jan-10	Narval	1222.735 34	05:37:58	4 × 600	1790	−3.126	−16.837	0.19	−2.3 ± 0.9	8.424×10^{-11}
τ Boo	25-Jan-10	Narval	1222.766 51	06:22:52	4 × 600	1590	−3.116	−16.825	0.22	−0.6 ± 1.0	2.225×10^{-06}
τ Boo	27-Jan-10	Narval	1224.646 86	03:30:20	4 × 600	1660	−2.549	−16.300	0.22	2.5 ± 1.0	6.221×10^{-05}
τ Boo	27-Jan-10	Narval	1224.714 61	05:07:53	4 × 600	1490	−2.528	−16.361	0.24	2.9 ± 1.1	3.485×10^{-02}
τ Boo	12-Feb-10	Narval	1240.595 80	02:14:58	4 × 600	1260	2.266	−16.041	0.34	1.0 ± 1.5	5.891×10^{-01}
τ Boo	13-Feb-10	Narval	1241.635 37	03:11:51	4 × 600	1020	2.580	−16.747	0.43	−1.0 ± 1.9	6.981×10^{-01}
τ Boo	13-Feb-10	Narval	1241.716 88	05:09:13	4 × 600	1130	2.605	−16.813	0.37	−2.2 ± 1.7	4.960×10^{-02}
τ Boo	14-Feb-10	Narval	1242.604 30	02:26:60	4 × 600	1570	2.872	−16.833	0.23	1.2 ± 1.0	7.482×10^{-05}
τ Boo	14-Feb-10	Narval	1242.717 37	05:09:49	4 × 600	1630	2.907	−16.737	0.21	−0.4 ± 0.9	5.608×10^{-09}
τ Boo	14-Jan-11	Narval	1576.701 36	04:50:25	4 × 600	1730	−2.267	−16.956	0.19	1.1 ± 0.9	9.118×10^{-04}
τ Boo	15-Jan-11	Narval	1577.690 79	04:35:04	4 × 600	1490	−1.968	−16.357	0.23	−0.4 ± 1.0	1.731×10^{-03}
τ Boo	16-Jan-11	Narval	1578.685 66	04:27:34	4 × 600	1840	−1.668	−16.057	0.18	−0.4 ± 0.8	2.920×10^{-01}
τ Boo	22-Jan-11	Narval	1584.679 61	04:18:07	4 × 600	1670	0.142	−16.147	0.20	−1.4 ± 0.9	5.847×10^{-01}
τ Boo	22-Jan-11	Narval	1584.709 97	05:01:50	4 × 600	1660	0.151	−16.126	0.20	−0.9 ± 0.9	8.562×10^{-02}
τ Boo	22-Jan-11	Narval	1584.740 32	05:45:32	4 × 600	1530	0.160	−16.117	0.22	−1.7 ± 1.0	6.900×10^{-01}
τ Boo	23-Jan-11	Narval	1585.688 04	04:30:08	4 × 600	1760	0.446	−16.390	0.18	0.8 ± 0.8	3.481×10^{-03}
τ Boo	23-Jan-11	Narval	1585.725 92	05:24:41	4 × 600	1860	0.458	−16.428	0.18	−0.3 ± 0.8	2.009×10^{-03}
τ Boo	23-Jan-11	Narval	1585.756 29	06:08:24	4 × 600	1810	0.467	−16.450	0.18	1.7 ± 0.8	2.857×10^{-05}
τ Boo	24-Jan-11	Narval	1586.664 87	03:56:39	4 × 600	1580	0.741	−17.000	0.23	−0.3 ± 1.0	2.588×10^{-03}
τ Boo	24-Jan-11	Narval	1586.695 230	04:40:22	4 × 600	1700	0.750	−16.995	0.20	−0.7 ± 0.9	8.092×10^{-03}
τ Boo	24-Jan-11	Narval	1586.725 580	05:24:05	4 × 600	1790	0.759	−16.993	0.19	0.5 ± 0.8	9.390×10^{-03}
τ Boo	25-Jan-11	Narval	1587.666 570	03:58:59	4 × 600	1780	1.043	−16.391	0.18	0.3 ± 0.8	3.947×10^{-01}
τ Boo	25-Jan-11	Narval	1587.696 930	04:42:42	4 × 600	1830	1.053	−16.362	0.18	−0.9 ± 0.8	9.800×10^{-02}
τ Boo	25-Jan-11	Narval	1587.727 280	05:26:24	4 × 600	1820	1.062	−16.336	0.18	−0.4 ± 0.8	8.442×10^{-03}
τ Boo	26-Jan-11	Narval	1588.674 650	04:10:30	4 × 600	930	1.348	−16.197	0.37	2.8 ± 1.6	5.712×10^{-01}
τ Boo	26-Jan-11	Narval	1588.705 000	04:54:12	4 × 600	1190	1.357	−16.211	0.28	0.0 ± 1.2	4.340×10^{-01}
τ Boo	26-Jan-11	Narval	1588.735 360	05:37:55	4 × 600	1650	1.366	−16.227	0.20	−0.4 ± 0.9	5.440×10^{-02}

Table A2. Journal of observations of four stars for which the magnetic field was detected and analysed.

Star	Date	Instrument	HJD (245 4000+)	UT time (h:m:s)	T_{exp} (s)	SNR	ϕ_{rot}	RV (km s^{-1})	σ_{LSD} ($10^{-4} I_c$)	B_l (G)	FAP
HD 73256	19-Jan-08	ESPaDOnS	484.897 43	09:24:56	4 × 560	410	−0.252	30.322	0.78	−2.6 ± 1.5	8.171×10^{-3}
HD 73256	21-Jan-08	ESPaDOnS	486.895 75	09:22:25	4 × 560	540	−0.109	29.997	0.56	1.0 ± 1.1	9.523×10^{-1}
HD 73256	22-Jan-08	ESPaDOnS	487.912 45	09:46:26	4 × 560	600	−0.036	30.313	0.51	5.3 ± 1.0	$<10^{-8}$
HD 73256	23-Jan-08	ESPaDOnS	488.950 53	10:41:13	4 × 700	540	0.038	29.858	0.57	4.2 ± 1.1	$<10^{-8}$
HD 73256	24-Jan-08	ESPaDOnS	489.948 60	10:38:24	4 × 780	700	0.109	30.302	0.43	0.5 ± 0.9	1.836×10^{-6}
HD 73256	25-Jan-08	ESPaDOnS	490.906 82	09:38:12	4 × 630	580	0.178	30.050	0.53	−1.4 ± 1.1	9.917×10^{-2}
HD 73256	27-Jan-08	ESPaDOnS	492.916 95	09:52:43	4 × 900	580	0.321	30.356	0.47	0.3 ± 0.9	$<10^{-8}$
HD 73256	28-Jan-08	ESPaDOnS	493.919 23	09:55:58	4 × 900	390	0.393	29.877	0.69	4.6 ± 1.4	$<10^{-8}$
HD 73256	30-Jan-08	ESPaDOnS	495.929 00	10:09:58	2 × 900	360	0.536	30.131	0.83	−0.7 ± 1.6	$<10^{-8}$
HD 102195	19-Jan-08	ESPaDOnS	484.957 47	10:54:30	4 × 540	270	−0.228	2.209	1.31	5.4 ± 2.4	$<10^{-8}$
HD 102195	20-Jan-08	ESPaDOnS	485.958 43	10:55:46	4 × 560	620	−0.145	2.112	0.51	6.3 ± 1.0	$<10^{-8}$
HD 102195	21-Jan-08	ESPaDOnS	486.953 69	10:48:49	4 × 560	560	−0.062	2.132	0.57	5.5 ± 1.2	$<10^{-8}$
HD 102195	22-Jan-08	ESPaDOnS	487.940 96	10:30:22	4 × 560	620	0.020	2.142	0.51	2.6 ± 1.1	5.1×10^{-5}
HD 102195	23-Jan-08	ESPaDOnS	489.098 31	14:16:50	4 × 780	680	0.117	2.101	0.46	2.2 ± 0.9	2.1×10^{-1}
HD 102195	24-Jan-08	ESPaDOnS	490.103 08	14:23:34	4 × 630	610	0.200	2.028	0.51	3.6 ± 1.1	1.3×10^{-5}
HD 102195	25-Jan-08	ESPaDOnS	490.938 14	10:25:58	4 × 630	500	0.270	2.119	0.65	3.3 ± 1.3	3.4×10^{-2}
HD 102195	27-Jan-08	ESPaDOnS	493.101 87	14:21:30	4 × 700	640	0.450	2.137	0.45	−1.1 ± 0.8	6.6×10^{-3}
HD 102195	28-Jan-08	ESPaDOnS	494.102 13	14:21:46	4 × 700	590	0.533	2.013	0.48	0.7 ± 1.0	5.1×10^{-6}
HD 102195	30-Jan-08	ESPaDOnS	496.090 29	14:04:31	4 × 800	440	0.699	2.164	0.63	5.5 ± 1.3	$<10^{-8}$
HD 46375	18-Jan-08	ESPaDOnS	483.842 91	08:06:50	4 × 215	460	0.245	−0.910	0.68	2.1 ± 0.9	$<10^{-8}$
HD 46375	19-Jan-08	ESPaDOnS	484.832 47	07:51:51	4 × 560	550	0.269	−0.912	0.56	2.4 ± 0.8	$<10^{-8}$
HD 46375	21-Jan-08	ESPaDOnS	486.833 95	07:54:05	4 × 560	670	0.317	−0.900	0.46	3.0 ± 0.6	$<10^{-8}$
HD 46375	22-Jan-08	ESPaDOnS	487.881 89	09:03:10	4 × 560	670	0.342	−0.953	0.46	3.1 ± 0.6	$<10^{-8}$
HD 46375	23-Jan-08	ESPaDOnS	488.911 50	09:45:52	4 × 780	770	0.366	−0.992	0.39	2.5 ± 0.5	$<10^{-8}$
HD 46375	24-Jan-08	ESPaDOnS	489.906 55	09:38:48	4 × 780	780	0.390	−0.920	0.39	3.0 ± 0.5	$<10^{-8}$
HD 46375	25-Jan-08	ESPaDOnS	490.872 63	08:50:01	4 × 630	770	0.413	−0.911	0.40	2.5 ± 0.5	$<10^{-8}$
HD 46375	26-Jan-08	ESPaDOnS	491.837 84	07:59:59	4 × 630	650	0.436	−0.956	0.43	2.7 ± 0.6	$<10^{-8}$
HD 46375	27-Jan-08	ESPaDOnS	492.793 08	06:55:35	4 × 800	690	0.459	−0.889	0.40	2.4 ± 0.5	$<10^{-8}$
HD 130322	20-Jan-08	ESPaDOnS	486.170 67	16:07:04	4 × 560	670	−0.059	−12.244	0.44	1.0 ± 1.1	4.482×10^{-4}
HD 130322	21-Jan-08	ESPaDOnS	487.170 20	16:06:14	4 × 560	620	−0.020	−12.292	0.48	2.3 ± 1.2	1.580×10^{-2}
HD 130322	22-Jan-08	ESPaDOnS	488.130 40	15:08:47	4 × 780	730	0.017	−12.332	0.42	1.9 ± 1.0	1.219×10^{-3}
HD 130322	23-Jan-08	ESPaDOnS	489.132 28	15:11:22	4 × 700	700	0.055	−12.342	0.43	3.2 ± 1.1	1.229×10^{-2}
HD 130322	24-Jan-08	ESPaDOnS	490.133 94	15:13:37	4 × 700	650	0.094	−12.304	0.47	1.7 ± 1.2	1.129×10^{-2}
HD 130322	25-Jan-08	ESPaDOnS	491.119 98	14:53:22	2 × 630	410	0.131	−12.227	0.68	−0.8 ± 1.7	5.418×10^{-1}
HD 130322	27-Jan-08	ESPaDOnS	493.134 65	15:14:12	4 × 700	610	0.209	−12.124	0.46	2.7 ± 1.1	$<10^{-8}$
HD 130322	28-Jan-08	ESPaDOnS	494.134 85	15:14:21	4 × 700	540	0.247	−12.124	0.51	3.2 ± 1.3	9.045×10^{-6}
HD 130322	30-Jan-08	ESPaDOnS	496.167 89	16:01:39	2 × 650	370	0.326	−12.213	0.77	5.9 ± 1.9	2.070×10^{-5}

Table A3. Journal of observations of four stars for which the magnetic field is not detected.

Star	Date	Instrument	HJD (245 4000+)	UT time (h:m:s)	T_{exp} (s)	SNR	ϕ_{rot}	RV (km s^{-1})	σ_{LSD} ($10^{-4} I_c$)
XO-3	14-Oct-09	ESPaDOnS	753.914 090	09:50:38	4 × 860	310	0.8911	−12.663	0.90
XO-3	14-Oct-09	ESPaDOnS	754.007 340	12:04:54	4 × 860	250	0.9156	−12.706	1.14
XO-3	14-Oct-09	ESPaDOnS	754.101 130	14:19:58	4 × (860	310	0.9403	−12.730	0.87
XO-3	15-Oct-09	ESPaDOnS	754.951 580	10:44:35	4 × 860	290	1.1641	−11.998	0.93
XO-3	15-Oct-09	ESPaDOnS	755.030 280	12:37:55	4 × 860	310	1.1848	−11.840	0.87
XO-3	15-Oct-09	ESPaDOnS	755.123 800	14:52:35	4 × 860	240	1.2094	−11.590	1.14
XO-3	16-Oct-09	ESPaDOnS	755.929 600	10:12:55	4 × 860	130	1.4215	−10.170	2.27
XO-3	16-Oct-09	ESPaDOnS	756.022 450	12:26:37	4 × 860	100	1.4459	−10.398	3.38
XO-3	16-Oct-09	ESPaDOnS	756.129 000	15:00:03	4 × 860	50	1.4739	−10.237	9.12
XO-3	17-Oct-09	ESPaDOnS	756.896 140	09:24:42	4 × 860	160	1.6758	−12.451	1.88
XO-3	17-Oct-09	ESPaDOnS	757.009 760	12:08:19	4 × 860	90	1.7057	−12.285	3.81
XO-3	18-Oct-09	ESPaDOnS	757.890 810	09:17:01	4 × 860	310	1.9376	−12.478	0.89
XO-3	18-Oct-09	ESPaDOnS	757.999 710	11:53:49	4 × 860	290	1.9662	−12.338	0.92
XO-3	18-Oct-09	ESPaDOnS	758.092 700	14:07:44	4 × 860	300	1.9907	−12.175	0.91
XO-3	19-Oct-09	ESPaDOnS	758.924 770	10:05:53	4 × 860	300	2.2097	−9.862	0.92
XO-3	19-Oct-09	ESPaDOnS	759.028 770	12:35:39	4 × 860	300	2.2370	−10.000	0.89
XO-3	19-Oct-09	ESPaDOnS	759.122 950	14:51:16	4 × 860	290	2.2618	−10.271	0.95
XO-3	20-Oct-09	ESPaDOnS	759.898 910	09:28:38	4 × 860	290	2.4660	−12.298	0.94

Table A3 – *continued*

Star	Date	Instrument	HJD (245 4000+)	UT time (h:m:s)	T_{exp} (s)	SNR	ϕ_{rot}	RV (km s^{-1})	σ_{LSD} ($10^{-4} I_c$)
XO-3	20-Oct-09	ESPaDOnS	759.987 590	11:36:20	4 × 860	290	2.4894	−12.440	0.93
XO-3	20-Oct-09	ESPaDOnS	760.076 200	13:43:56	4 × 860	290	2.5127	−12.540	0.94
HAT-P-2	26-Jun-07	ESPaDOnS	277.780 050	06:38:01	4 × 900	470	0.6472	−19.115	0.55
HAT-P-2	27-Jun-07	ESPaDOnS	278.797 830	07:03:38	4 × 800	500	0.9082	−19.254	0.51
HAT-P-2	28-Jun-07	ESPaDOnS	279.793 500	06:57:25	4 × 900	500	1.1635	−19.490	0.51
HAT-P-2	01-Jul-07	ESPaDOnS	282.791 670	06:54:50	4 × 900	500	1.9322	−19.164	0.53
Corot-7	05-Jan-10	Narval	1202.515 870	24:15:19	4 × 2000	120	52.9038	31.264	3.08
Corot-7	06-Jan-10	Narval	1203.495 410	23:45:52	4 × 2000	80	53.2805	31.226	4.87
Corot-7	18-Jan-10	Narval	1215.489 870	23:38:10	4 × 2000	90	57.8938	31.234	4.73
Corot-7	27-Jan-10	Narval	1224.459 390	22:54:42	4 × 2000	130	61.3436	31.188	2.87

This paper has been typeset from a TEX/LATEX file prepared by the author.